

Two Black Boxes, One Solver: Encoder Probing and Decoder Attribution for Neural Multi-Attribute VRP under Hard-Mask and Recourse Decoders

Sohaib Afifi

Univ. Artois, UR 3926, Laboratoire de Génie Informatique et d'Automatique de l'Artois (LGI2A),
F-62400 Béthune, France
sohaib.afifi@univ-artois.fr

Abstract

Neural autoregressive solvers for the Multi-Attribute Vehicle Routing Problem (MAVRP) reach competitive cost but offer no per-step justification, a problem when dispatchers must validate, accept, or compare them. We open two complementary black boxes in one protocol. On the *encoder* side, linear probes, spontaneous-organization metrics, rank-based richness measures, and discovered-direction analyses with intervention validation characterize how the latent represents constraint families at the graph, node, and edge level. On the *decoder* side, three attribution methods (gradient, integrated gradients, DeepLIFT) feed three reading angles: abductive, contrastive against the best feasible alternative, and counterfactual (smallest input change that switches the action or restores feasibility). Explanations are scored on fidelity, concentration, stability, sanity, and actionability. Across six variants combining three encoders (ATT baseline, UNIMP, UNIMPMOE) with two decoders (HARD-MASK, RECURSE), we find that graph inductive bias improves both representational predictability and decoder sanity, that the Mixture-of-Experts encoder represents constraints in a distributed rather than axis-aligned way, and that the RECURSE training regime, not merely its softer mask, produces policies that represent infeasibility usefully, exposing make-feasible counterfactuals that HARD-MASK policies fail to produce even when fed infeasible alternatives externally.

1 Introduction

The Multi-Attribute Vehicle Routing Problem (MAVRP) packs several VRP variants into a single combinatorial problem: a single instance can simultaneously activate capacity, time-window, distance-limit, backhaul, and open-route constraints [Kool *et al.*, 2019; Berto *et al.*, 2024]. Neural autoregressive solvers built on attention [Vaswani *et al.*, 2017; Kool *et al.*, 2019] or graph encoders such as UniMP [Shi *et al.*, 2021], optionally with conditional compute through a Mixture-of-Experts (MoE) layer [Shazeer *et al.*, 2017], now match strong heuristics on these benchmarks, including graph-based unified models built specifically for MAVRP [Jari *et al.*, 2025]. They remain, however, opaque: at every decoding step the policy emits an action with no exposed justification of which inputs mattered, which constraints dominated, which alternative was close, or what minimal change would have flipped the decision.

This opacity is an operational liability rather than a purely epistemic one. Logistics dispatchers need (i) *diagnosis* of anomalous routes, (ii) *validation* against explicit business rules, (iii) *acceptability* of the solver's recommendations, and (iv) *comparability* between candidate solver families. These four needs cut across both representation and decision: an encoder may legibly encode a constraint that the decoder ignores, and a decoder may attribute mass to a feature whose representation is degenerate. We therefore argue that neural CO solvers require a *joint* XAI account of both stages, evaluated on the same checkpoints with a shared grid.

We make four contributions. First, we propose a two-pillar protocol that probes the encoder for predictability, spontaneous organization, richness, and discovered directions, while attributing decoder decisions through three complementary reading angles. Second, we introduce a constraint-family taxonomy that aggregates raw input gradients into operations-readable groups (capacity/demand, geometry, time windows, route-recourse). Third, we apply the protocol to six MAVRP solver variants combining three encoder families (ATT baseline, UNIMP, UNIMPMOE) with two decoder variants (HARD-MASK and RECURSE) and report under five XAI criteria. We deliberately compare a strong-mask decoder (HARD-MASK, feasibility-by-construction) against a weak-mask decoder (RECURSE, feasibility-by-learning) because the gap is itself the contribution: the recourse decoder is the only one in which “why was this alternative not chosen?” has a non-trivial answer, and where *make-feasible* counterfactuals can exist at all. Fourth, we expose phenomena invisible to inference cost alone: distributed coding in UNIMPMOE, sanity gap between ATT and the graph encoders, and a representational gap between HARD-MASK and RECURSE policies that make-feasible counterfactuals reveal even after we control for the mask.

2 Setup

Problem. An instance of MAVRP is a directed graph $G = (V, E)$ with one depot and n customers. Each customer carries linehaul/backhaul demands, a service time, and a time window; each instance carries a vehicle capacity, an optional distance limit, and a flag for open routes. Following the unified parameterization of [Berto *et al.*, 2024] we sample instances such that any subset of constraint families may be active, so the same encoder–decoder pair must handle every variant. We use $n = 50$ customers throughout.

Solver family. The policy π_θ first encodes the whole instance into per-node embeddings $h \in \mathbb{R}^{n \times d}$, then autoregressively decodes a permutation by attending over the masked candidate set. We compare three encoders: ATT, a Transformer-style attention encoder used as the *baseline* architecture; UNIMP, a graph encoder with structural inductive bias [Shi *et al.*, 2021; Jari *et al.*, 2025]; UNIMPMOE, the same backbone augmented with a Mixture-of-Experts layer for conditional compute [Shazeer *et al.*, 2017].

Decoder variant. We pair every encoder with two decoder variants that differ only in how feasibility is delivered. The HARD-MASK decoder enforces every active constraint (capacity, time windows, distance, backhaul, open-route) directly in the action mask: only feasible candidates ever reach the softmax, so feasibility is guaranteed by construction. The RECOURSE decoder masks only already-visited customers and leaves the policy itself to learn the constraints; infeasible selections are allowed during training and pay a recourse cost in the reward, and the decoder is given per-step state features (remaining capacity, time slack, recourse cost) so it can become aware of constraint slack at decoding time. Both share the same attention-masked autoregressive backbone, so the comparison isolates the effect of how feasibility is delivered. The six (encoder \times decoder) checkpoints are the unit of comparison throughout the paper.

3 Method

We instrument both stages of the trained policy and score every output on a single five-criterion grid. The protocol is implemented as a batch runner that consumes a checkpoint and returns a structured report combining encoder probes, decoder attributions, and evaluation metrics. We run three seeds per (encoder \times decoder \times method) cell over 128 instances.

3.1 Encoder Probing

We ask four questions of the frozen latent h , all answered at the graph, node, and edge level.

Predictability. Can the active constraint families be linearly recovered from h ? We train per-family linear probes [Alain and Bengio, 2017] and report ROC-AUC for binary indicators and macro-F1 for multi-class targets. Two complementary unsupervised readouts are computed on PCA/ICA components of h : an *axis-unique* score (best correlation with a single component) and a *top- k subspace* score (best correlation with a k -dimensional subspace). The gap between the two diagnoses distributed coding: information that lives across components rather than along a single axis.

Spontaneous organization. Without labels, k -means on h should partition instances by constraint family. We score the partition with silhouette [Rousseeuw, 1987], NMI [Vinh *et al.*, 2010], and ARI [Hubert and Arabie, 1985], and visualise it with t-SNE [van der Maaten and Hinton, 2008].

Richness. The effective rank and stable rank of h [Roy and Vetterli, 2007] detect collapse to a low-dimensional subspace and serve as denominators in the rank-vs-organization synthesis (Figure 2).

Discovered directions. PCA and ICA decompositions of h produce candidate latent axes; we then align each axis with a known reference bank of constraint indicators and concept descriptors. To validate the resulting alignments causally, we intervene along each direction in the latent and check whether the targeted concept moves in the predicted direction (*intervention validation*); we also measure the across-seed stability of these directions.

3.2 Decoder Attribution: Three Reading Angles

At decoding step t the policy emits logits $u_{t,a}$ over the masked candidate set; let $a_t = \arg \max_a u_{t,a}$ be the chosen action and a'_t the best feasible alternative. We attribute every step with three input attribution methods (gradient, integrated gradients [Sundararajan *et al.*, 2017], and DeepLIFT [Shrikumar *et al.*, 2017]) using Captum [Kokhlikyan *et al.*, 2020].

Abductive. For each method we obtain an input-attribution tensor $g_{i,f}$ at step t , then aggregate it to per-node $s_i = \sum_f |g_{i,f}|$, per-feature $s_f = \frac{1}{N} \sum_i |g_{i,f}|$, and per-constraint-family $s_{\text{fam}} = \sum_{f \in \text{fam}} s_f$. The top- k on each level answers “*why this action?*”.

Contrastive. We compute the margin $\Delta_t = u_{t,a_t} - u_{t,a'_t}$ and attribute $\partial \Delta_t / \partial x_{i,f}$. Features whose contrastive attribution is largest are those that *depart* the chosen action from its closest feasible rival. The margin $|\Delta_t|$ also doubles as a confidence signal: a large value indicates a clear preference, a small value a tight call.

Counterfactual. A directed search guided by the contrastive gradient looks for the smallest input perturbation that either (i) flips the chosen action (*switch*) or (ii) restores feasibility for an infeasible alternative (*make-feasible*). Both modes test *actionability*: can a dispatcher reach a different decision through a small, plausible change to the instance? We specify the search fully rather than tune it. It runs only when a feasible alternative a'_t exists and the margin $\Delta_t = u_{t,a_t} - u_{t,a'_t}$ is finite and positive, and ranges over a fixed dictionary of seven signed relaxations, each pushing a binding constraint the way that helps: node-level time-window end (\uparrow), service time (\downarrow), linehaul and backhaul demand (\downarrow), and instance-level vehicle capacity, distance limit and depot time-window end (\uparrow). For each candidate c the first-order step $\delta_c = \Delta_t / |\partial \Delta_t / \partial x_c|$ estimates the change that closes the margin; we discard it if the gradient points the wrong way, if the move is inadmissible (e.g. a value below zero), or if its relative size $\delta_c / \max(|x_c|, 1)$ exceeds a $5\times$ budget cap. The three smallest survivors are verified by applying the move (with a 5% overshoot) and replaying one decode step, recording a switch if a'_t becomes the $\arg \max$ or a make-feasible

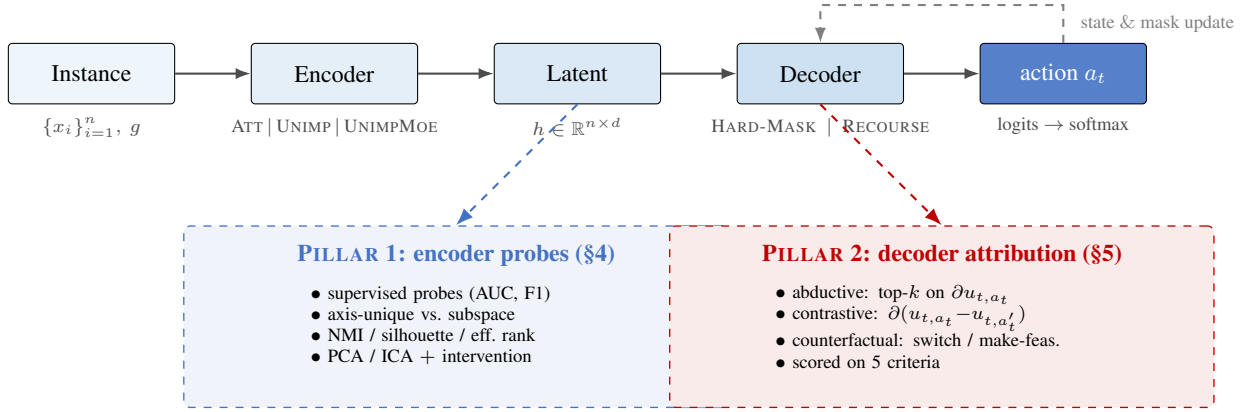


Figure 1: Solver pipeline (top row) and the two XAI pillars. The pipeline encodes the instance into a per-node latent h and autoregressively decodes a permutation; the dashed gray arrow is the action loop: at every step t the chosen a_t updates the decoder state and the feasibility mask before the next decision. PILLAR 1 probes the frozen latent (§4); PILLAR 2 attributes the per-step action under three reading angles, scored on five criteria (§5). Both pillars share the same six (encoder family \times decoder variant) checkpoints, so all comparisons are made on the same trained policies.

if the infeasible a'_t turns feasible; we return the first success, else the smallest attempt. The search is thus deterministic with a fixed budget of three replays, so the rates in §5.7 are lower bounds a larger budget could only raise.

3.3 Five-Criterion Evaluation

Each criterion answers one operational question; we state what it measures and what a dispatcher reads from it. For each (model, method) we report:

- **Fidelity:** *do the highlighted inputs really drive the decision?* A deletion test perturbs the top- k attributed nodes and measures the action flip rate ($flip@k$) and log-probability drop ($\Delta logp@k$); a faithful explanation flips the action when its own top nodes are removed.
- **Concentration:** *focused or diffuse?* $focus@k$ is the mass on the top- k features and $clarity$ is one minus the normalised entropy of the attribution, so a sharp story scores high and a smeared one low.
- **Stability:** *would a differently seeded model tell the same story?* We re-run the attribution on independently seeded checkpoints of the same variant and measure agreement on the top node ($node@1$), top-3 set ($node@3$, Jaccard), dominant family ($family$), and best alternative ($alt.$); this is the standard reproducibility-under-retraining notion, quantified in Table 6.
- **Sanity:** *learned saliency or architectural artefact?* The ratio of $flip@1$ between the trained policy and a randomised-weight copy, after [Adebayo *et al.*, 2018]: a ratio near one means the attribution survives destroying the weights and cannot be trusted.
- **Actionability:** *can a small instance change reach a different decision?* The counterfactual availability rate (any switch or make-feasible found) and the make-feasible rate.

The same grid applies to all (model, method) pairs, including the ATT baseline. Because no prior joint encoder–decoder

Model	NMI	macro-F1	route-open F1	flow-struct F1	eff-rank	silhouette
ATT / HARD-MASK	0.48	0.23	0.48	0.94	14.4	0.36
ATT / RECOURSE	0.50	0.22	0.50	0.94	14.2	0.39
UNIMP / HARD-MASK	0.57	0.36	1.00	0.93	15.7	0.19
UNIMP / RECOURSE	0.67	0.50	1.00	0.95	15.3	0.24
UNIMP MOE / HARD-MASK	0.55	0.36	1.00	0.91	15.95	0.20
UNIMP MOE / RECOURSE	0.64	0.43	0.99	0.97	15.5	0.22

Table 1: Graph-level encoder summary. NMI / macro-F1 of k -means signatures vs. constraint families; F1 on two illustrative families; effective rank; best silhouette over k .

XAI protocol for neural CO solvers exists to benchmark against, the grid carries its own controls: the randomised-weight policy is the negative control for every attribution criterion (§5.5), and the ATT/HARD-MASK cell (un-graph encoder, feasibility-by-construction decoder) is the reference against which the graph-bias and recourse effects are read.

4 Encoder Results

4.1 Predictability and Distributed Coding

Table 1 reports the supervised picture. Both graph encoders dominate ATT on signature NMI (0.55–0.67 vs. 0.48–0.50) and on multi-class macro-F1 (0.36–0.50 vs. 0.22–0.23). They reach the ceiling on simple binary indicators (*e.g.* route openness, 1.00 vs. 0.48–0.50). Pairing the graph encoders with the RECOURSE decoder adds another 0.05–0.14 on NMI on top of either HARD-MASK pairing, so the ranking is stable: UNIMP/RECOURSE \succ UNIMP MOE/RECOURSE \succ either HARD-MASK variant of the graph family \succ ATT.

The unsupervised PCA/ICA readouts add a more nuanced picture. Read on a single dominant axis, UNIMP MOE underperforms UNIMP on several constraint families. As soon as we allow a top- k subspace, UNIMP MOE catches up to within ~ 0.04 of UNIMP. The implication is that UNIMP MOE does not encode *less* information; it encodes it in a more distributed, non-axis-aligned way. Without the second readout, a researcher would conclude that UNIMP MOE is a worse encoder than UNIMP; with it, the difference is one of representational geometry, not capacity.

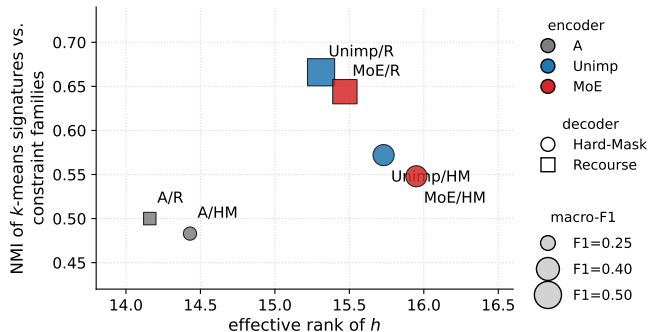


Figure 2: Joint reading of the encoder pillar. X : effective rank of h . Y : NMI of k -means signatures with constraint families. *Point size*: multi-class macro-F1 of the constraint probe. Color encodes encoder family; marker encodes decoder variant. ATT sits at the bottom-left with small markers; UNIMP/RECOURSE dominates on organization and F1; UNIMP/MOE is rich and distributed.

4.2 Spontaneous Organization and Richness

Even without supervision the latent organises by constraint family. NMI of k -means signatures (Table 1) ranks the encoders in the same order as the supervised probes, but the absolute values are higher than what the silhouette score alone would suggest, which is why combining both metrics is necessary. ATT wins on silhouette (0.36–0.39, vs. 0.19–0.24 for the graph encoders): its clusters are tight but smaller and less informative.

Effective rank and stable rank tell a complementary story. The graph encoders use a measurably wider portion of their representation space (UNIMP ~ 15.7 , UNIMP/MOE ~ 15.95) than ATT (~ 14.4), without collapse. Plotted jointly with NMI (Figure 2), the picture is unambiguous: ATT at the bottom-left, UNIMP leading on organization, UNIMP/MOE leading on richness while remaining well organised. A single-metric reading would have hidden the rank-organization trade-off.

4.3 Concepts, Nodes, and Edges

Moving from raw constraint indicators to constructed concepts (compactness, clustering, outliers, capacity pressure, combined tension) flattens the ranking: concept macro-F1 sits at 0.56–0.60 across all six variants, ATT slightly ahead on a few binary concepts. The graph advantage is thus on the raw constraint skeleton, not on derived concepts. The picture also changes with granularity. At the *node* level the graph encoders still lead (node-role macro-F1 0.62–0.64 vs. 0.57–0.59, widest on route position). At the *edge* level it inverts on one informative axis: *same-route* prediction is high across all encoders (AUC 0.90–0.92), with ATT on par or slightly above; attention encodes pairwise relational structure as well as a graph encoder does, even when its global summary is less organised. The graph advantage is therefore not uniform: it concentrates on global structure and per-node role, not on pairwise relational bookkeeping.

Method	mean gap	best on
OR-Tools	1.94%	0
MTPOMO	2.45%	0
MVMoE	2.29%	0
CaDA	1.71%	6
ATT / HARD-MASK	1.82%	0
UNIMP / HARD-MASK	1.54%	0
UNIMP/MOE / HARD-MASK	1.39%	10
ATT / RECOURSE	2.87%	0
UNIMP / RECOURSE	2.91%	0
UNIMP/MOE / RECOURSE	2.78%	0

Table 2: Inference cost across 16 MAVRP variants at $n = 50$ (gap-to-BKS averaged, “best on” counts the variants where the method wins). HARD-MASK checkpoints reach published-baseline level; UNIMP/MOE/HARD-MASK tops the grid. RECOURSE checkpoints pay an explicit $\sim 1\%$ gap for their interpretability properties.

4.4 Discovered Directions and Intervention

PCA and ICA decompositions of h surface candidate latent axes. Aligning each axis against the known reference bank (Figure 3), several principal components correlate strongly with one or two constraint families: route openness, geometry, and capacity pressure are recoverable from the leading axes, while time-window-related families remain spread over multiple components. This is qualitative evidence that the encoder’s leading directions are interpretable without supervision, which we then test causally.

Intervention validation (Figure 4) pushes each aligned axis in the latent and checks whether the targeted concept moves in the predicted direction. Concept-level success is 1.00 on all six variants, confirming that the alignments carry causal weight. Direction-level success is more modest at 0.48–0.59, with PCA correlations small or negative for UNIMP and UNIMP/MOE, in line with the distributed-coding result of §4.1: the linear axis used for the intervention captures only part of the underlying signal in the GNN latents. Stability across seeds confirms that the leading axes themselves are reliable artefacts of the trained encoder, not of the random PCA/ICA initialisation.

5 Decoder Results

5.1 Inference Cost: the Solvers Are Competitive

Before reading the XAI signal, it matters that the policies under study are actually competitive. Table 2 reports the mean gap-to-BKS across 16 MAVRP variants at $n = 50$, alongside the published learning baselines [Berto *et al.*, 2024]. The HARD-MASK checkpoints land in the 1.39–1.82% band, matching or beating every published baseline (UNIMP/MOE/HARD-MASK wins outright on 10 of 16 variants and CaDA on 6). The RECOURSE checkpoints sit at 2.73–2.91%, roughly 1 point worse than their HARD-MASK counterparts and on the same order as MTPOMO/MVMoE. The cost is therefore an explicit trade-off: RECOURSE buys the interpretability properties documented below at a measurable but bounded gap penalty. This rules out the alternative reading in which RECOURSE “looks more interpretable” simply because its policy is degenerate.

PCA discovered component correlations with known banks (grouped by encoder)

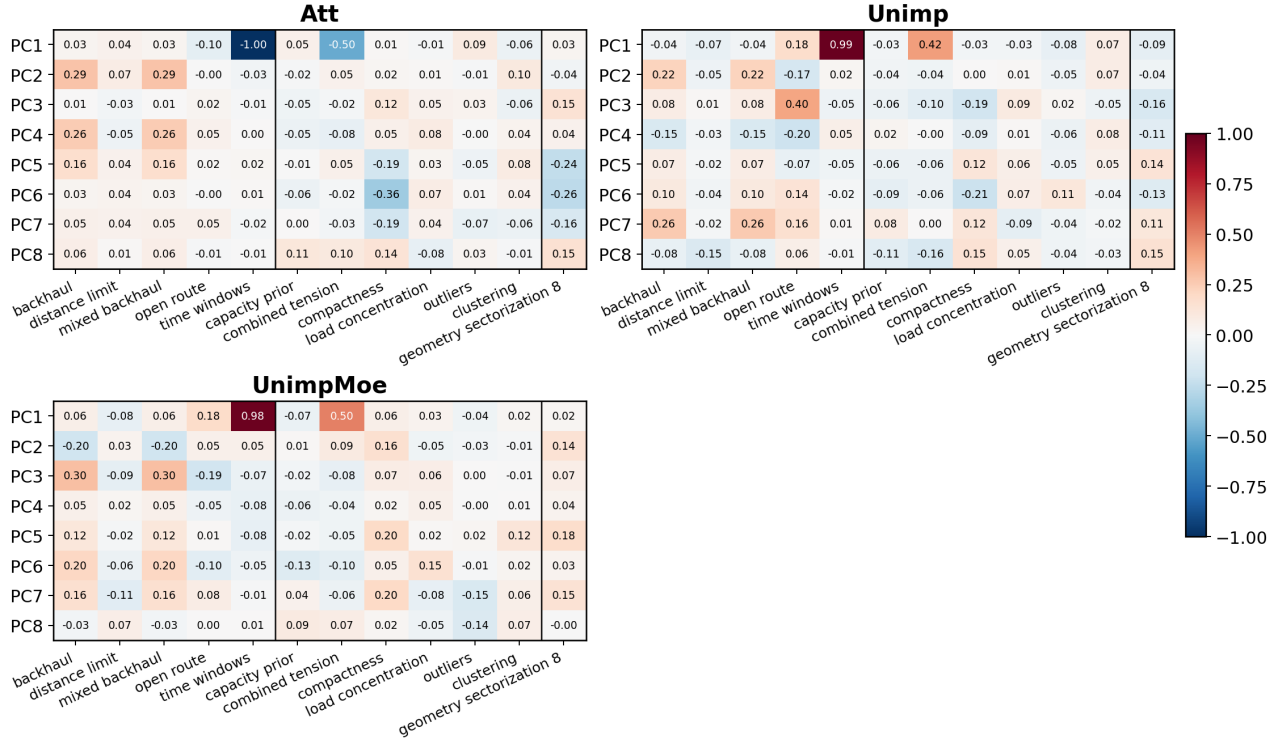


Figure 3: Alignment of the leading PCA components with the known constraint-and-concept bank, one panel per encoder family (each averages that family’s two decoder variants). Rows are components PC1–PC8; columns are constraint indicators (left group) and derived concepts (right group); a cell is the signed correlation between the component and the reference, red positive, blue negative. Read the leading rows: ATT’s PC1 locks onto route openness (−1.00) while the graph encoders’ PC1 locks onto time windows (~ 0.98); the remaining constraints spread across several components, the distributed pattern quantified in §4.1.

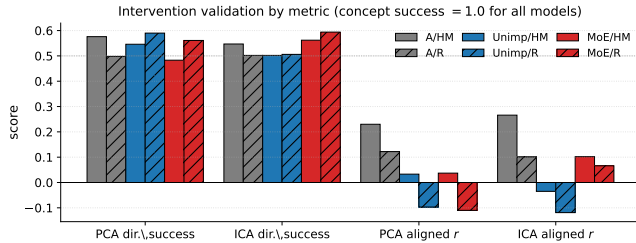


Figure 4: Intervention validation grouped by metric: directional success (PCA / ICA) and aligned-perturbation correlation (PCA / ICA). Bars within each metric compare the six (encoder × decoder) variants. Hatched bars are RECURSE decoders; bar color is the encoder family. Concept-level success is 1.0 for all variants and is omitted.

5.2 Constraint Families that Drive Decisions

Figure 5 reports the average constraint-family share of attribution mass. Two patterns emerge. First, the dominant family is *method-sensitive*: gradient favours capacity/demand for ATT (~ 60%) and geometry for UNIMP/UNIMP MOE; integrated gradients flips this to time-windows for ATT (> 40%) and geometry for the graph encoders (> 50%); DeepLIFT pushes the largest share into the dynamic decoder-state “other” bucket, especially under RECURSE. The qualita-

Model	alt. rate	Δlogit	Δlogp
ATT / HARD-MASK	0.74	2.01	9.92
ATT / RECURSE	0.81	1.82	8.54
UNIMP / HARD-MASK	0.75	2.21	9.74
UNIMP / RECURSE	0.86	2.24	9.82
UNIMP MOE / HARD-MASK	0.76	1.99	9.21
UNIMP MOE / RECURSE	0.83	2.29	9.55

Table 3: Contrastive readout. “alt. rate” = fraction of steps with at least one feasible alternative; Δ is the chosen-vs-alternative margin.

tive reading thus depends on the method; this is evidence for a multi-criterion grid, not a flaw of any single attribution. Second, the RECURSE decoder inflates the “other” bucket (route-recourse and dynamic decoder-state features) by ~ 7–11 points under gradient/IG and ~ 20 under DeepLIFT: it shifts the decision horizon off raw inputs and onto its running state. The three methods therefore agree on the *regime effect* even while disagreeing on the *family ranking*.

5.3 Contrastive: Recourse Exposes More Alternatives

Table 3 shows that the alternative-availability rate climbs from 0.74–0.76 under the HARD-MASK decoder to 0.81–

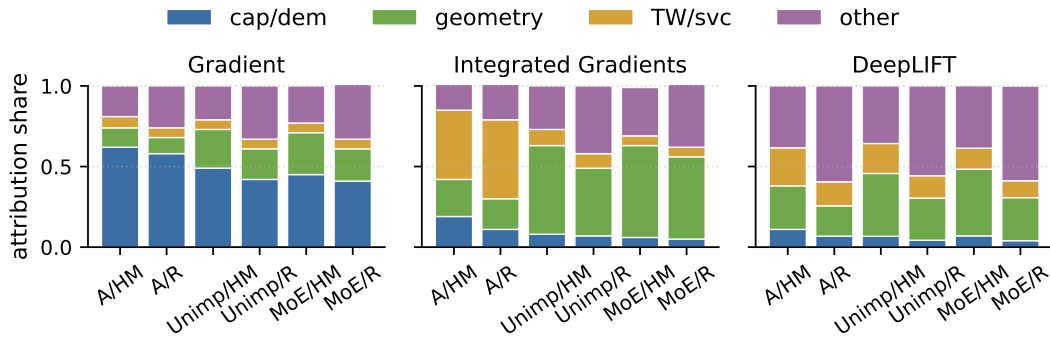


Figure 5: Stacked attribution share over the four constraint families, by (encoder \times decoder), under gradient, integrated gradients, and DeepLIFT (left to right). The three methods agree on the RECOURSE decoder shifting mass into “other” but disagree on the dominant family, which is what motivates a multi-criterion grid.

Model	flip@1	flip@3	flip@5	$\Delta\text{logp}@1$	$\Delta\text{logp}@3$
ATT / HARD-MASK	0.471	0.509	0.521	6.37	4.56
ATT / RECOURSE	0.474	0.499	0.518	6.00	3.62
UNIMP / HARD-MASK	0.468	0.474	0.474	7.28	5.29
UNIMP / RECOURSE	0.518	0.537	0.560	8.01	5.40
UNIMP MOE / HARD-MASK	0.463	0.493	0.510	7.15	5.27
UNIMP MOE / RECOURSE	0.487	0.497	0.527	7.41	4.93

Table 4: Deletion faithfulness (gradient method, trained weights). UNIMP/RECOURSE leads on every metric; the worst-best gap on flip@5 is ~ 9 points.

0.86 under the RECOURSE decoder, across all three encoders. The RECOURSE decoder systematically widens the local choice set without inflating the margin: gaps stay tight at ~ 2 logits, meaning many decisions are close calls, the setting in which contrastive explanations are most informative. Note that the contrastive readout is method-independent: it only requires knowing the chosen action and the next-best feasible candidate.

5.4 Faithfulness

Table 4 reports the deletion-faithfulness numbers for the gradient method. Perturbing the single most-attributed node already flips the decision in $\sim 47\text{--}52\%$ of steps, and the log-prob drop is consistently larger for the graph encoders ($\Delta\text{logp}@1$ 7.15–8.01) than for ATT (6.00–6.37). UNIMP/RECOURSE leads on every metric. The choice of attribution method barely moves faithfulness: averaged over all six variants, gradient, integrated gradients, and DeepLIFT stay within 0.02 of each other on flip@1 and within 0.20 on $\Delta\text{logp}@3$. They are equally faithful even though they disagree on which family they highlight (Figure 5): equal-fidelity attributions can tell different qualitative stories, which is exactly why the scorecard separates fidelity from concentration.

5.5 Sanity

Table 5 contrasts trained and randomized weights. All encoders pass: trained policies flip more often and the log-prob drops are an order of magnitude larger. Strikingly, the trained/random ratio on flip@1 is $\sim 1.7\times$ for ATT but $\sim 3.5\text{--}$

Encoder	flip@1		ratio	$\Delta\text{logp}@1$	
	trained	random		trained	random
ATT	0.47	0.27	$\sim 1.7\times$	6.18	0.01
UNIMP	0.49	0.12	$\sim 4.2\times$	7.65	-0.32
UNIMP MOE	0.47	0.14	$\sim 3.5\times$	7.28	-0.40

Table 5: Sanity check: trained vs. randomized-weight policies (gradient method). Graph encoders pass much more decisively than ATT.

Model	node@1	node@3	family	alt.
ATT / HARD-MASK	0.504	0.514	0.985	0.509
ATT / RECOURSE	0.512	0.519	0.948	0.508
UNIMP / HARD-MASK	0.517	0.512	0.808	0.506
UNIMP / RECOURSE	0.520	0.518	0.627	0.515
UNIMP MOE / HARD-MASK	0.509	0.521	0.894	0.509
UNIMP MOE / RECOURSE	0.504	0.516	0.631	0.505

Table 6: Cross-seed stability (gradient method): mean agreement of explanations across independently seeded checkpoints of the same variant, over all $\binom{4}{2} = 6$ seed pairs. *node@1 / node@3*: agreement on the top attributed node / top-3 node set (Jaccard); *family*: agreement on the dominant constraint family; *alt.*: agreement on the identified best alternative. Higher is more reproducible.

$4.2\times$ for the graph encoders. Part of ATT’s saliency is therefore architectural rather than learned, a finding only the sanity criterion exposes, and one which would silently bias a head-to-head comparison restricted to flip@ k alone.

5.6 Stability

Stability is the pillar most easily asserted and least often measured, so we quantify it directly. Table 6 re-runs the gradient attribution on four independently seeded checkpoints of each variant and reports how often the explanations agree across the six seed pairs. Node-level saliency reproduces only moderately and uniformly: the top node agrees about half the time (*node@1* 0.50–0.52), the top-3 set overlaps similarly (*node@3* 0.51–0.52), and the named best alternative shows the same near-tie (*alt.* ~ 0.51). This floor is expected: many nodes carry comparable mass and the margins are tight (~ 2

logits, §5.3), so the exact ranking is seed-sensitive even when the story is not.

The dominant *family* is far more reproducible, and how reproducible is itself informative. ATT and the HARD-MASK policies pin the same family almost every time (0.95–0.99 for ATT; 0.81–0.89 for UNIMP/UNIMP/MOE under HARD-MASK), whereas the graph encoders under RECOURSE fall to ~ 0.63 . This mirrors the constraint-share result (§5.2): when a policy spreads its decision onto distributed decoder-state features, *which* family reads as dominant is less determined and flips more across seeds. The property that makes RECOURSE explanations richer thus makes their one-line family summary less stable, a trade-off a fidelity-only reading would hide. The pattern is method-robust: IG and DeepLIFT give the same ~ 0.50 node floor and family agreement in the 0.63–0.85 band.

5.7 Counterfactuals and Make-Feasible

The search finds at least one switch or make-feasible candidate at 32–49% of steps, with UNIMP/RECOURSE on top (0.49). The *make-feasible* mode has rate 0.00 for all three HARD-MASK decoders and 0.03–0.06 for all three RECOURSE decoders, and RECOURSE’s perturbations are smaller (0.82–1.23 vs. 1.03–1.46): smaller and more frequent. By itself the asymmetry is mechanical (HARD-MASK masks infeasible candidates out by construction, so the search has nothing to operate on), which raises the real question: could the HARD-MASK *policy* produce make-feasible counterfactuals if we lifted that restriction? We test this next.

Representational ablation. To isolate the policy effect from the mask effect, we re-ran the search on the three HARD-MASK checkpoints with the alt-selector externally widened to the visited-only candidate pool, the same pool RECOURSE sees at training. The widened alt-availability rate matches the RECOURSE regime (0.88, 0.72, 0.86 for ATT, UNIMP, UNIMP/MOE), yet the make-feasible rate *stays* at 0.00 across all three encoders. The HARD-MASK policy was never trained to assign meaningful logit mass to infeasible candidates, so the next-best alternative the alt-selector returns is almost always already feasible and the perturbation has nothing to re-feasibilize. The HARD-MASK vs. RECOURSE make-feasible gap is therefore a property of the trained policy, not of the mask: training under recourse cost is what produces a policy whose counterfactual neighbourhood contains actionable make-feasible moves.

5.8 Scorecard

Figure 6 folds the eight headline metrics into one heatmap. It covers four of the five criteria (fidelity, concentration, sanity, actionability) as per-checkpoint columns; the fifth, stability, is a cross-seed quantity reported separately in Table 6. UNIMP/RECOURSE wins on five of the eight metrics, including faithfulness and counterfactual availability, and ATT/HARD-MASK wins on none; the RECOURSE rows are uniformly greener than the HARD-MASK rows, except on $\Delta\text{logp}@3$. Read with the stability table the picture is nuanced rather than a clean sweep: RECOURSE buys richer, more actionable explanations at the cost of a less stable single-family

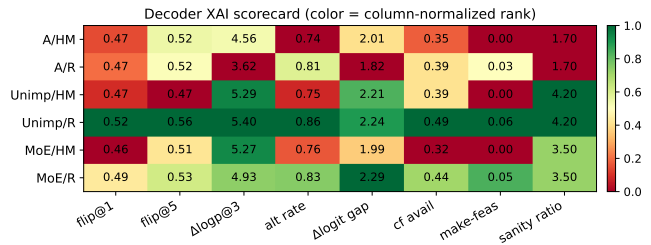


Figure 6: Decoder XAI scorecard across eight metrics covering fidelity, contrast, actionability, and sanity. Color is column-normalized rank; cell text is the raw value.

summary. The scorecard makes both the encoder ranking and the decoder effect visible at a glance, which is what an operations team needs from a comparability tool.

6 Related Work

Linear probing of frozen representations [Alain and Bengio, 2017] is standard for linear decodability; we extend it to structural MAVRP constraints and add axis-unique vs. subspace readouts to expose distributed coding. Gradient, integrated gradients [Sundararajan *et al.*, 2017], and DeepLIFT [Shrikumar *et al.*, 2017] via Captum [Kohli *et al.*, 2020] are mature in vision/NLP but rarely combined on neural CO solvers; we adopt the sanity protocol of [Adebayo *et al.*, 2018] as the criterion that flags architecturally-induced saliency. GNNExplainer [Ying *et al.*, 2019] and attention-flow methods [Abnar and Zuidema, 2020] target a single forward pass on a static graph, whereas we attribute autoregressive *actions* whose state evolves with each decision, forcing the per-step contrastive reading. Classical counterfactuals seek the smallest input change that flips a class; the *make-feasible* mode (smallest change that turns an infeasible alternative feasible) is, to our knowledge, specific to recourse-style policies with no direct analogue in classification XAI.

7 Discussion and Conclusion

What XAI revealed. Architecture matters for both representation and decision. Graph inductive bias lifts probe quality, sharpens spontaneous organization, and passes the sanity check more decisively; and the MoE encoder is not less informative than UNIMP but represents constraints in a distributed subspace, visible only beyond axis-aligned probes. None of this could be read off the inference cost alone.

Decoder matters. The RECOURSE decoder widens the contrastive landscape and shifts attribution toward dynamic decoder-state features; crucially, its *training regime* is what produces a policy whose neighbourhood contains make-feasible counterfactuals, which the HARD-MASK policy fails to produce even when fed infeasible alternatives externally. The decoder is therefore not just a performance choice but an *interpretability* choice: it changes what kind of explanation the solver can produce at all.

Scale robustness. On all six $n = 100$ checkpoints the gradient-method picture holds: graph encoders lead ATT on

faithfulness ($\Delta \log p @ 1$ up to 10.7 vs. 8.9–9.5), RECOURSE widens the contrastive landscape (alt rate 0.89–0.91 vs. 0.84–0.85), and the make-feasible asymmetry is textbook (0.03 for every RECOURSE, 0.00 for every HARD-MASK). The protocol is not overfit to $n = 50$.

Limits and outlook. Three limits scope the claims: the encoder pillar relies on a *supervised* concept dictionary, so it tests only for structure we thought to name; the counterfactual search is a first-order, fixed-budget proposal (§3.2), so its rates are lower bounds a heavier optimiser would raise; and the $n = 100$ check uses one seed per cell, so only the $n = 50$ grid is variance-controlled. Four directions follow: (i) *dispatcher-in-the-loop* evaluation in the spirit of HCXAI, measuring whether operators diagnose, accept, or override routes faster with the explanations in hand; (ii) a stability-regularised or multi-family attribution that resolves the stability–richness trade-off we surface (§5.4); (iii) porting the make-feasible counterfactual to other recourse-trained policies (scheduling, bin packing, soft-constrained dispatching) to test how VRP-specific the effect is; and (iv) growing this grid and its controls into the standard XAI benchmark neural CO still lacks. The protocol is reproducible on any MAVRP checkpoint trained with the rl4co interface [Berto *et al.*, 2024].

References

- [Abnar and Zuidema, 2020] Samira Abnar and Willem Zuidema. Quantifying attention flow in transformers. In *ACL*, 2020.
- [Adebayo *et al.*, 2018] Julius Adebayo, Justin Gilmer, Michael Muelly, Ian Goodfellow, Moritz Hardt, and Been Kim. Sanity checks for saliency maps. In *NeurIPS*, 2018.
- [Alain and Bengio, 2017] Guillaume Alain and Yoshua Bengio. Understanding intermediate layers using linear classifier probes. In *ICLR Workshop*, 2017. arXiv:1610.01644.
- [Berto *et al.*, 2024] Federico Berto, Chuanbo Hua, Junyoung Park, Laurin Luttman, Yining Ma, Fanchen Bu, Jiarui Wang, Haoran Ye, Minsu Kim, Sanghyeok Choi, André Hottung, Jianan Zhou, Jieyi Bi, Yu Hu, Fei Liu, Hyeonah Kim, Jiwoo Son, Haeyeon Kim, Wouter Kool, Zhiguang Cao, Jie Zhang, Kijung Shin, Cathy Wu, Sungsoo Ahn, Guojie Song, Changhyun Kwon, Lin Xie, and Jinkyoo Park. RL4CO: An extensive reinforcement learning for combinatorial optimization benchmark. In *NeurIPS Datasets and Benchmarks*, 2024.
- [Hubert and Arabie, 1985] Lawrence Hubert and Phipps Arabie. Comparing partitions. *Journal of Classification*, 2:193–218, 1985.
- [Jari *et al.*, 2025] Amine Jari, Sohaib Afifi, Rym Nesrine Guibadj, and Eric Lefèvre. G-UniRouting: A graph-based unified neural model for solving multi-attribute vehicle routing problems. In *2025 IEEE 37th International Conference on Tools with Artificial Intelligence (ICTAI)*, pages 491–498. IEEE, 2025.
- [Kokhlikyan *et al.*, 2020] Narine Kokhlikyan, Vivek Miglani, Miguel Martin, Edward Wang, Bilal Alsallakh, Jonathan Reynolds, Alexander Melnikov, Natalia Kliushkina, Carlos Araya, Siqi Yan, and Orion Reblitz-Richardson. Captum: A unified and generic model interpretability library for PyTorch. *arXiv preprint arXiv:2009.07896*, 2020.
- [Kool *et al.*, 2019] Wouter Kool, Herke van Hoof, and Max Welling. Attention, learn to solve routing problems! In *ICLR*, 2019.
- [Rousseeuw, 1987] Peter J. Rousseeuw. Silhouettes: A graphical aid to the interpretation and validation of cluster analysis. *Journal of Computational and Applied Mathematics*, 20:53–65, 1987.
- [Roy and Vetterli, 2007] Olivier Roy and Martin Vetterli. The effective rank: A measure of effective dimensionality. In *EUSIPCO*, 2007.
- [Shazeer *et al.*, 2017] Noam Shazeer, Azalia Mirhoseini, Krzysztof Maziarz, Andy Davis, Quoc Le, Geoffrey Hinton, and Jeff Dean. Outrageously large neural networks: The sparsely-gated mixture-of-experts layer. In *ICLR*, 2017.
- [Shi *et al.*, 2021] Yunsheng Shi, Zhengjie Huang, Shikun Feng, Hui Zhong, Wenjing Wang, and Yu Sun. Masked label prediction: Unified message passing model for semi-supervised classification. In *IJCAI*, 2021.
- [Shrikumar *et al.*, 2017] Avanti Shrikumar, Peyton Greenside, and Anshul Kundaje. Learning important features through propagating activation differences. In *ICML*, 2017.
- [Sundararajan *et al.*, 2017] Mukund Sundararajan, Ankur Taly, and Qiqi Yan. Axiomatic attribution for deep networks. In *ICML*, 2017.
- [van der Maaten and Hinton, 2008] Laurens van der Maaten and Geoffrey Hinton. Visualizing data using t-SNE. *Journal of Machine Learning Research*, 9:2579–2605, 2008.
- [Vaswani *et al.*, 2017] Ashish Vaswani, Noam Shazeer, Niki Parmar, Jakob Uszkoreit, Llion Jones, Aidan N. Gomez, Lukasz Kaiser, and Illia Polosukhin. Attention is all you need. In *NeurIPS*, 2017.
- [Vinh *et al.*, 2010] Nguyen Xuan Vinh, Julien Epps, and James Bailey. Information theoretic measures for clusterings comparison: Variants, properties, normalization and correction for chance. *Journal of Machine Learning Research*, 11:2837–2854, 2010.
- [Ying *et al.*, 2019] Rex Ying, Dylan Bourgeois, Jiaxuan You, Marinka Zitnik, and Jure Leskovec. GNNExplainer: Generating explanations for graph neural networks. In *NeurIPS*, 2019.